First results of asteroseismic exercise from Meudon

Błażej L. Popielski, Marie-Jo Goupil

Abstract

We present an application of the classic seismological forward problem in the context of solar-like oscillations. The range and quality of input frequency data are similar to those anticipated for observations from future space missions. The project is part of *hare and hound* exercise of the COROT SWG[1]. We focus on the possibility of reproducing p-mode spectra. However, we emphasize also the importance of mixed modes for sounding the deep interior.

1 Introduction

There is a strong need to reproduce the pulsational behavior of distant stars after the success of helioseismology. High quality spectra are being obtained as a result of months of dedicated satellite observations (Baglin, 1998). Investigating the solar-like oscillations is the first step for asteroseismology. While the number of detected frequencies is expected to be significantly lower than for the sun, blind experiments *(hare and hound* exercise) between independent groups have been undertaken. This work is the result of one of the groups working with two sets of frequencies.

In Section 2, we present the rules of the exercise concerning building a model and its oscillation frequencies. Next, we concentrate on accompanying the reader through the whole data analysis process. In Section 3 we focus on a simulated spectrum to reduce the number of important parameters. We describe then our forward method and present the resulting models which are believed to represent best the investigated observed frequency data (Section 4.).

2 Exercise rules

A set of artificial "observed" noise-free frequencies gives us opportunity to check our ability to find a solar-type model reproducing frequencies. The rules are based on what realistic conditions we hope to obtain for each target star of specific mission (see Provost, 2001). The assumptions of the *hare and hound* exercise concerning model (called observations starting from this point) refer to

[1] Latest news available at http://dasgal1.obspm.fr/~michel/COROT-SISMO.html.

ranges in metal abundance (Z/X) and HR-diagram parameters (T_{eff}, $L/L_{\odot}$). The ranges are as follows:

$$
\begin{gathered}
Z/X \in [0.019, 0.03], \\
\log T_{eff} \in [3.806, 3.82], \\
\log L/L_{\odot} \in [0.83, 0.89].
\end{gathered}
$$

The frequency set includes low degree ($\ell \leq 3$) modes, and contain rotationally split components ($m \neq 0$). There are 5 modeling parameters in game: mass, M, hydrogen abundance, X, metal abundance, Z, mixing length parameter, α, and overshoot parameter, d_{ov}. The mean spectral accuracy predicted for COROT mission is ~ 0.1 μHz, however it may vary from one mode to other (Baglin, 1998). We try to reproduce the spectra with predicted frequency accuracy.

In this work, we deal with two sets of artificial data.

3 Spectral analysis

3.1 Echelle diagram

One-to-one frequency separation histogram (Figure 1.) reveals main regular spacings in the spectrum. The main sinusoidal shape (with period of ~ 50 μHz) is due to the mean separation of two consecutive multiplets of equal spherical degree, ℓ. We find frequencies of $\ell = 0, 1, 2, 3$ modes on a spectral distance of this size. This distance is approximately equal to the mean large separation[2], $\langle D \rangle = \frac{1}{N} \sum_{n,\ell} D_{n\ell}$, where $D_{n\ell} = \nu_{n\ell 0} - \nu_{n-1\ell 0}$. It is basis of so-called echelle diagram (Grec, 1981). Echelle diagram is result of cutting the spectrum into such pieces and arranging them one above another. The frequency, ν, and the echelle-diagram coordinates, ν_{offset} and ν_{cut}, are related by following formulas,

$$
\begin{gathered}
\nu_{offset} = \nu - \nu_{cut}, \\
\nu_{cut} = \nu^0_{cut} + k \langle D \rangle,
\end{gathered}
$$

where two constants, $\langle D \rangle$ and ν^0_{cut}, need to be specified and k is an integer. While $\langle D \rangle$ is the signature of the mean density (thus the age), ν^0_{cut} has no physical meaning. It is fixed *a priori* for visualization purposes.

However, there are also fine structure peaks in the frequency separation histogram. They are due to the rotational splitting of the modes. The frequencies of $m = 0$ modes, i.e. centroids, may be distinguished in Figure 2. In order to focus on those frequencies we have to reduce equidistant frequencies of same radial order for all spherical degrees (Figure 3.). Figure 3. is an echelle diagram of observations and a model, as well. Each of the two sets consists of 4 branches of adiabatic frequencies of different spherical degree. The branches are similar curves. Model frequencies are present in adiabatic and non-adiabatic versions.

[2]Several groups use geometric mean instead of the arithmetic one. We quote here the one we used.

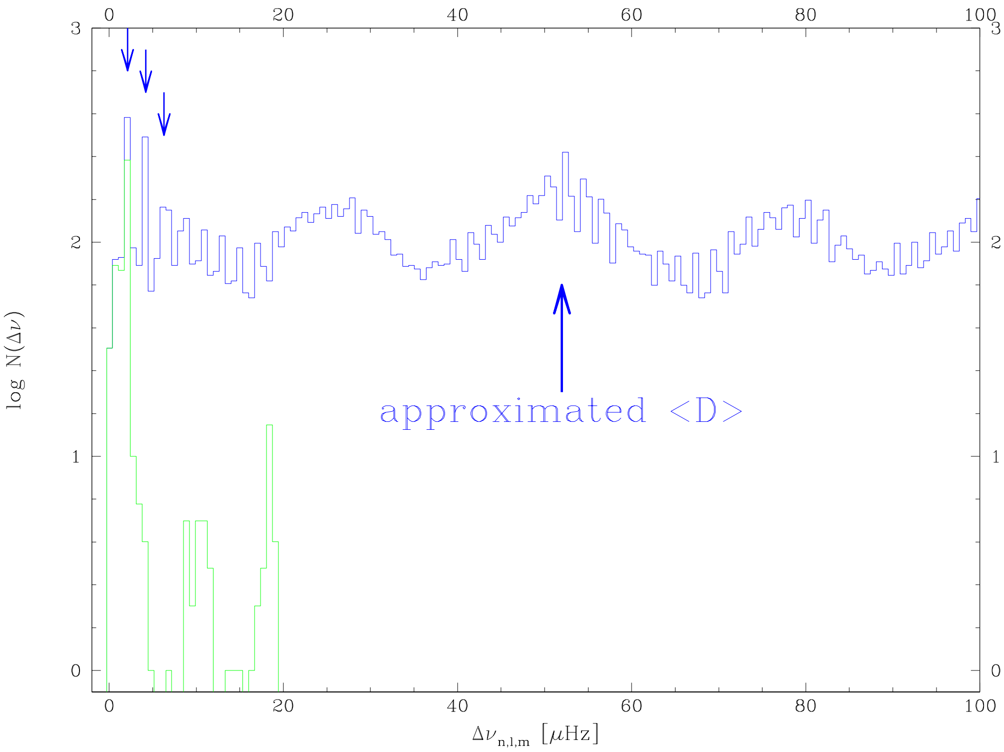

Figure 1: Frequency separation histograms for `set1`. Two curves relate to two separation sets, one-to-one separations (blue) and separations between two consecutive frequencies (green). The last-mentioned reveals two main peaks: one for rotational splitting ($\sim 2.1\ \mu$Hz) almost uniform for all modes and the multiplet frequency separation ($\sim 18.3\ \mu$Hz).

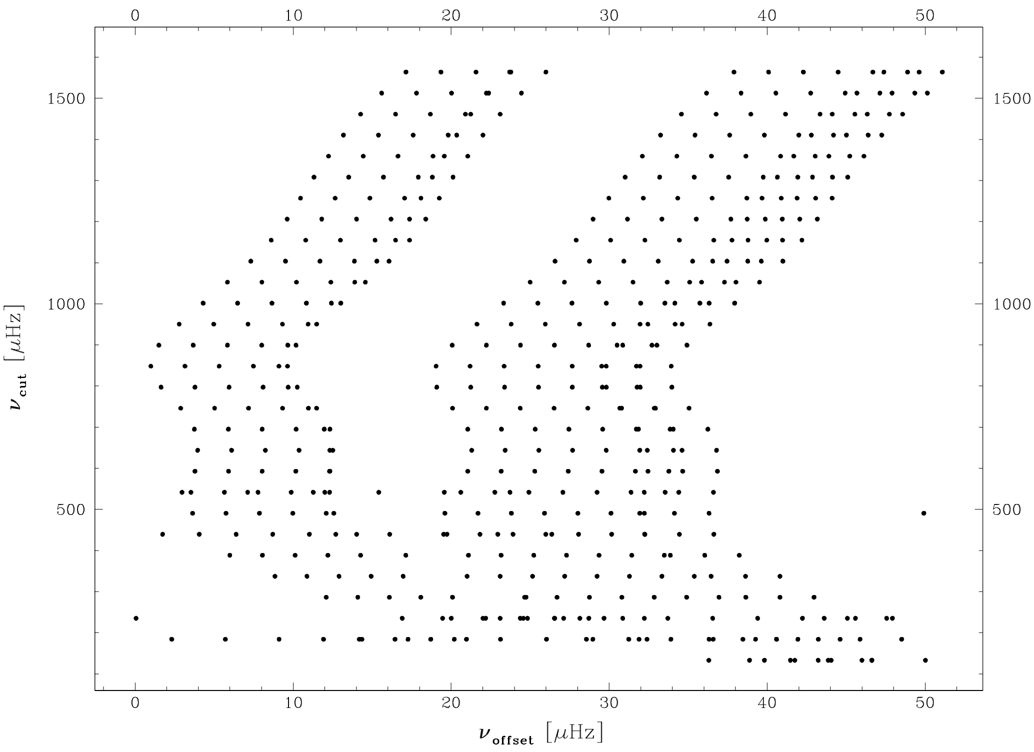

Figure 2: Echelle diagram for observed frequencies (`set1`). Most of horizontal frequency counts give 16. It is the sum of four multiplets of low spherical degree. Equidistant frequencies let us find appropriate ℓ. Lower part of the diagram is dominated by the mixed-modes. Their interpretation is much harder, while the don't obey asymptotic relations. Originate could be easily rescaled to fit radial degree.

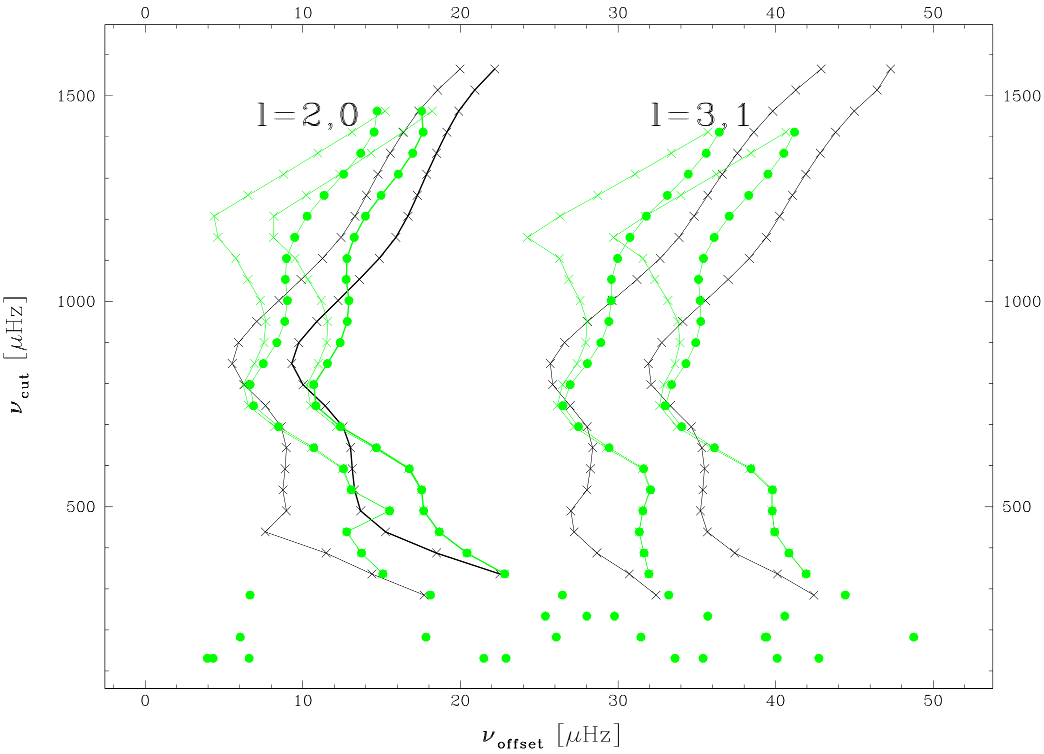

Figure 3: Same as in Figure 3. stripped of the rotational splitting. Observational frequencies are shown (black x), as well as adiabatic and non-adiabatic frequencies of a model (green dots and crosses, respectively). Observed radial mode branch is bold.

In the high frequency domain non-adiabatic corrections perturb the model spectra in an important way. We expect to reproduce real observational data, once available. However, there are certain important spectral signatures in this frequency region reveals. For this reason, we focus on $[400, 1400]$ μHz frequency domain. Lower frequency limit omits g-mode domain, where the asymptotic behavior is hard to encounter. On the other hand the acoustical cutoff frequency gives the upper limit (~ 1500 μHz). We keep in mind however that some of high frequencies from that domain may be also polluted.

3.2 Spectral parameters

The mean large frequency separation ,$\langle D \rangle$, is the crucial spectral parameter. It is sensitive to the mean stellar density However, it is one of many (see Figure 3.). It is a convenient diagnostic parameter, but in this work, we use mean offset frequency (echelle abscissa) for centroids of radial modes, $\left\langle \nu^0_{offset} \right\rangle$, where

$$\nu_{n0} = \nu^0_{cut} + k \langle D_0 \rangle + \nu^0_{offset}(\nu_{n0}).$$

This quantity is more practical for the purpose of frequency reproduction, while the mean large separation corresponds to its derivative and in fact some of frequency information is lost.

In this work we define and make use of 9 spectral parameters in total:

- $\left\langle \nu^0_{offset} \right\rangle$, mean offset frequency for radial mode branch at fixed ν^0_{cut},
- $(\nu_1, \Delta\nu_1)$, $(\nu_2, \Delta\nu_2)$, $(\nu_3, \Delta\nu_3)$, $(\nu_4, \Delta\nu_4)$, extreme points of reduced echelle diagram for $\ell = 0$ branch, see Figure 4.

The echelle diagram reduction, we use, is done by subtracting low, i.e. 3rd, order polynomial fitted to the observations, $\widetilde{\nu}^0_{offset}(\nu)$, from the standard echelle data, $\nu^0_{offset}(\nu)$,

$$\Delta\nu^0_{offset} = \nu^0_{offset}(\nu) - \widetilde{\nu}^0_{offset}(\nu).$$

This procedure brings to light small changes in the echelle diagram. These are subtle but the most significant changes and still surpass the error magnitude. We emphasize that you need to reproduce the 9 spectral parameters with an appropriate model.

4 Model search

The mean large separation diminishes with age of a star on the main sequence. The change of the mean offset frequency at constant ν^0_{cut} is quite more complicated. However it is only the matter of modeling ability, to reproduce $\left\langle \nu^0_{offset} \right\rangle$ with certain accuracy for a model of chosen ZAMS parameters. The impact

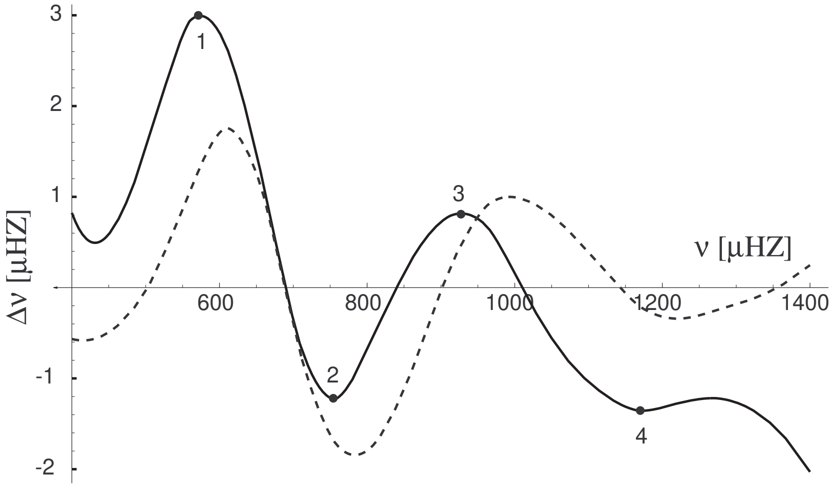

Figure 4: Reduced echelle diagram (see text) for a model (solid) and observations (dashed). The four extreme points serve their coordinates to characterize spectra.

of 5 such parameters on a model constructed in this manner is shown in Figure 5. Although large separation is used, 5 model parameters may be divided into those shifting spectral features (bumps) to higher ($M/M_{\odot}$, d_{ov}) and lower frequencies (X, Z, α). This behavior of each of the parameters change when models quit MS.

Note that we expect to find appropriate model on the cooling part of the track, because the ratio of the lifetime on the heating to that on the cooling part is about 0.5.

If we consider series of n models representing vicinity of a departure model, we result in series of spectral characteristics:

$$\{\nu_1^{(1)}, \nu_2^{(1)}, \nu_3^{(1)}, \nu_4^{(1)}, \Delta\nu_1^{(1)}, \Delta\nu_2^{(1)}, \Delta\nu_3^{(1)}, \Delta\nu_4^{(1)}\},$$

$$...$$

$$\{\nu_1^{(n)}, \nu_2^{(n)}, \nu_3^{(n)}, \nu_4^{(n)}, \Delta\nu_1^{(n)}, \Delta\nu_2^{(n)}, \Delta\nu_3^{(n)}, \Delta\nu_4^{(n)}\}.$$

If the range of those parameters encompasses corresponding observational values, $\{\nu_1^{(o)}, \nu_2^{(o)}, \nu_3^{(o)}, \nu_4^{(o)}, \Delta\nu_1^{(o)}, \Delta\nu_2^{(o)}, \Delta\nu_3^{(o)}, \Delta\nu_4^{(o)}\}$, we interpolate to find out model parameters. We are able to approach the observations using this method repeated in an iterative way. This method is quite demanding from numerical point of view. It is however clear that quality of interpolation reduces number of necessary iterations.

We carried all stellar modeling with Warsaw evolutionary code with high quality equation of state (Rogers, Swenson & Iglesias, 1996) and opacity tables (Rogers & Iglesias, 1996). Grain and molecular opacities were adopted as well as conductive ones. The burning rates were based on Bahcall (1995).

In our search we used 5 parameter interpolation. Thus, we had to choose 5 spectral parameters to solve the set of 5 equations, in order to reproduce the observed ones. We find it useful to deal with ν_1, ν_2, ν_3, $(\Delta\nu_1 - \Delta\nu_4)$ and $(\Delta\nu_3 - \Delta\nu_2)$. The effect of 3rd order in each modeling parameter was taken into account. We benefited the Mathematica(TM) 3.0 calculating engine to provide interpolation and the solution as well.

It should be stressed that this method is constraint independent. There is uniqely the shape of the radial mode ($\ell = 0$) branch of echelle diagram which is reproduced. It is obvious however that the resulting models (or their lack) depend on the departure model. It is recommended to start iterations from several departure models.

4.1 Model choice criteria

Once several iterative searches are done we may obtain several models that fit well. We have to choose one model spectra that fits best. We consider this is the one reproducing the most of frequencies. To be precise, for each frequency of a model we calculate its distance to the closest observed one, $\left|\nu_{n\ell}^{model} - \nu_{n\ell}^{obs}\right|$.

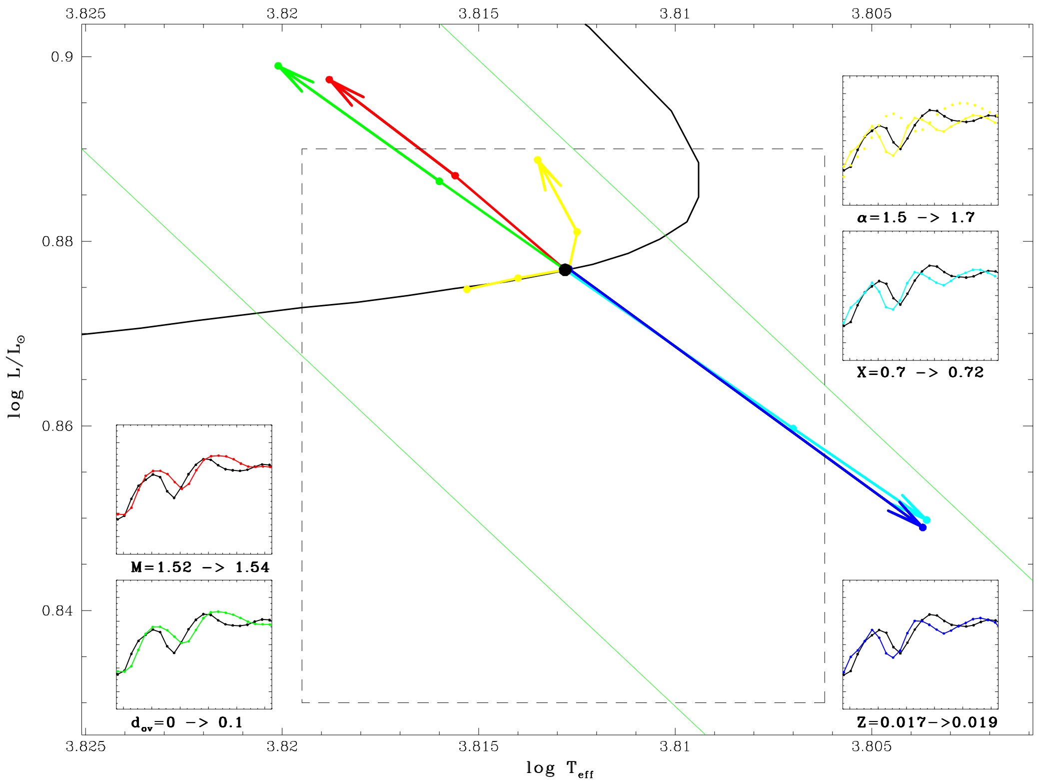

Figure 5: HR diagram showing the effects of ZAMS parameters. The arrows connect models with only one parameter changed. All the models have the observational $\left\langle \nu^0_{offset} \right\rangle$. The dashed box indicates the HR diagram *hare and hound* domain. The insets, $D_0(\nu)$, show the parameter influence on the $\ell = 0$ spectrum. Green lines are constant radius lines. The evolutionary track is also drawn (black line).

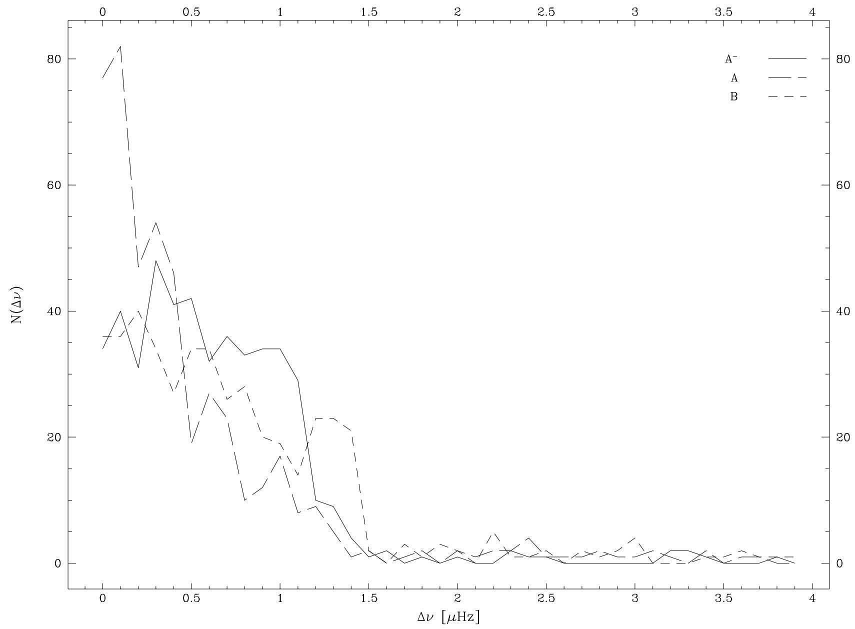

Figure 6: Histograms of differences between two spectra. 3 model spectra are compared with the observed one. $A^{-}$and A are following evolutionary models spectra. A model is the one with correct $\left\langle \nu^0_{offset} \right\rangle$ and also the one shown in Figure 3. B is a 1.5 $M_\odot$ model.

Histogram of such distances $N(k\delta\nu, (k+1)\delta\nu)$, for $k \geq 0$ and $\delta\nu \ll \nu^{obs}$, contains an unbiased and frequency-free information on the spectral fit. Next, we fit

$$f(\Delta\nu) = a_1 \exp(-a_2 \Delta\nu)$$

function to the histogram. Figure 6. presents 3 histograms data for models. Comparison of well-fitted spectra is in that way reduced to comparing a_1 and a_2 values for different models. While the number of compared frequencies is the same, it is $a_1$or a_2, that let us choose: the greater – the better fit.

The table below together with the Figure 6. let us distinguish the difference between "χ^2 minimum" and "histogram" criteria.

model	χ^2	a_1	a_2
A-	8.160	50.7	1.02
A	8.525	100	81.94
B	2.709	44.6	0.96

model	$M/M_\odot$	X	Z	α	d_{ov}	a_1
C	1.52	0.722	0.0175	1.7	0.04	10.17
D	1.525	0.71	0.019	1.67	0.02	8.78
E	1.363	0.703	0.0122	1.728	0.2	6.93

model	t [10^9yr]	X_c	$\log L/L_\odot$	$\log T_{eff}$	r_c/R
C	1.908	0.172	0.828	3.8142	0.058
D	1.770	0.170	0.830	3.8148	0.058
E	2.333	0.246	0.823	3.8216	0.062

Table 1: Model parameters from spectral fit to `set1`.

4.2 Search results

The goal was to find parameters of a model reproducing observed frequencies. As mentioned earlier, for our analysis we used two sets of artificial observations. The first one (`set1`) is an intergroup data. Its true parameters are unknown for us. The second one (`set2`) is an auxiliary one. It was generated by one of us and analysed by the other one. Its parameters were kept hidden until the end of analysis. In Table 1. we quote three models being results of three independent iterations for `set1`. There is visibly no perfect model found. For those 3 models, parameters span widely. However using our a_1-criteria we can choose the best (C).

The `set1` data was provided with frequency errors. Thus, we are allowed to compare the errors with spectral differences for models C, D, E and `set1` (Figure 7.).

Tabularized models lay outside the HR box of the *hare and hound* exercise. It could be the effect of modeling physics (equation of state, burning rates etc.) but certain general ease of reproducing radial branch could be the cause, as well. We incline to the second scenario, thus we suggest the need of reproducing also other quantities, apart from those of radial mode branch. Small separations and $f_n = \nu_{n1} - \nu_{n0}$ separations should do. In Figure 8. we present large, small and f_n separations for `set1` and a model.

There is however another set of constraints for the models. This is the set of frequencies of mixed-modes. In case of `set2` we had an opportunity to verify its applicability, while two mixed-modes are present in the set. They are modes captured during their avoided crossing event. They propagate in the envelope and in the convective core as well, thus their frequencies are important to be reproduced, as far as deep interior is concerned. Frequencies of those modes rise with age because of rising Brunt-Väisälä frequency at the edge of shrinking hydrogen core.

In our analysis those additional observables were simply frequencies of two mixed-modes. They were incorporated among 5 parameters of the interpolation procedure, described in Section 4. The iteration was carried as described earlier, except several steps that were enriched in the "mixed" parameters. Result of

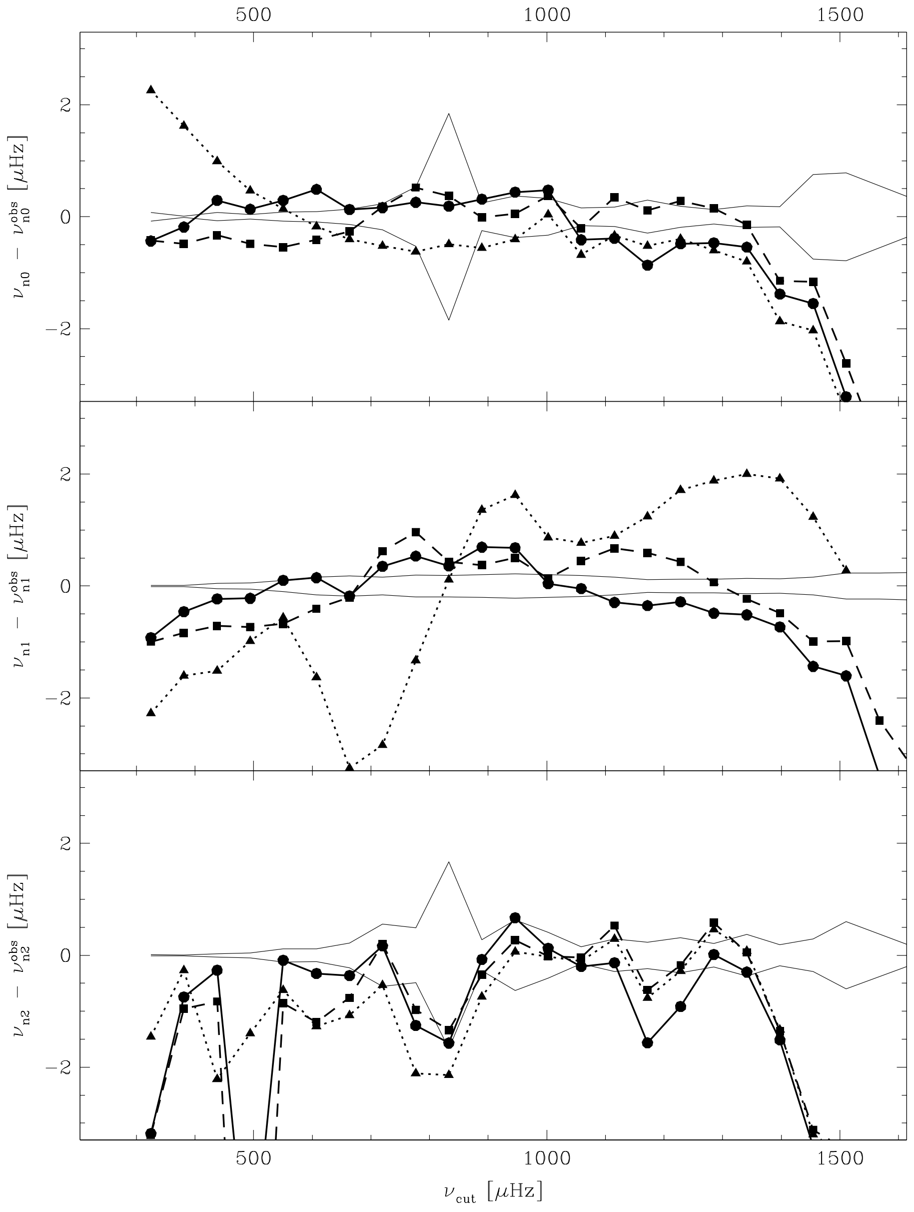

Figure 7: Frequencies of 3 fitted models from Table 1. relative to the observed frequencies. Each diagram corresponds to modes of one spherical degree, ℓ. Each model is shown with different line and pointstyles, C – solid line and circles, D – dashed line and squares, E – short dashed line and triangles. Symmetrical horizontal solid curves relate observed frequency errors.

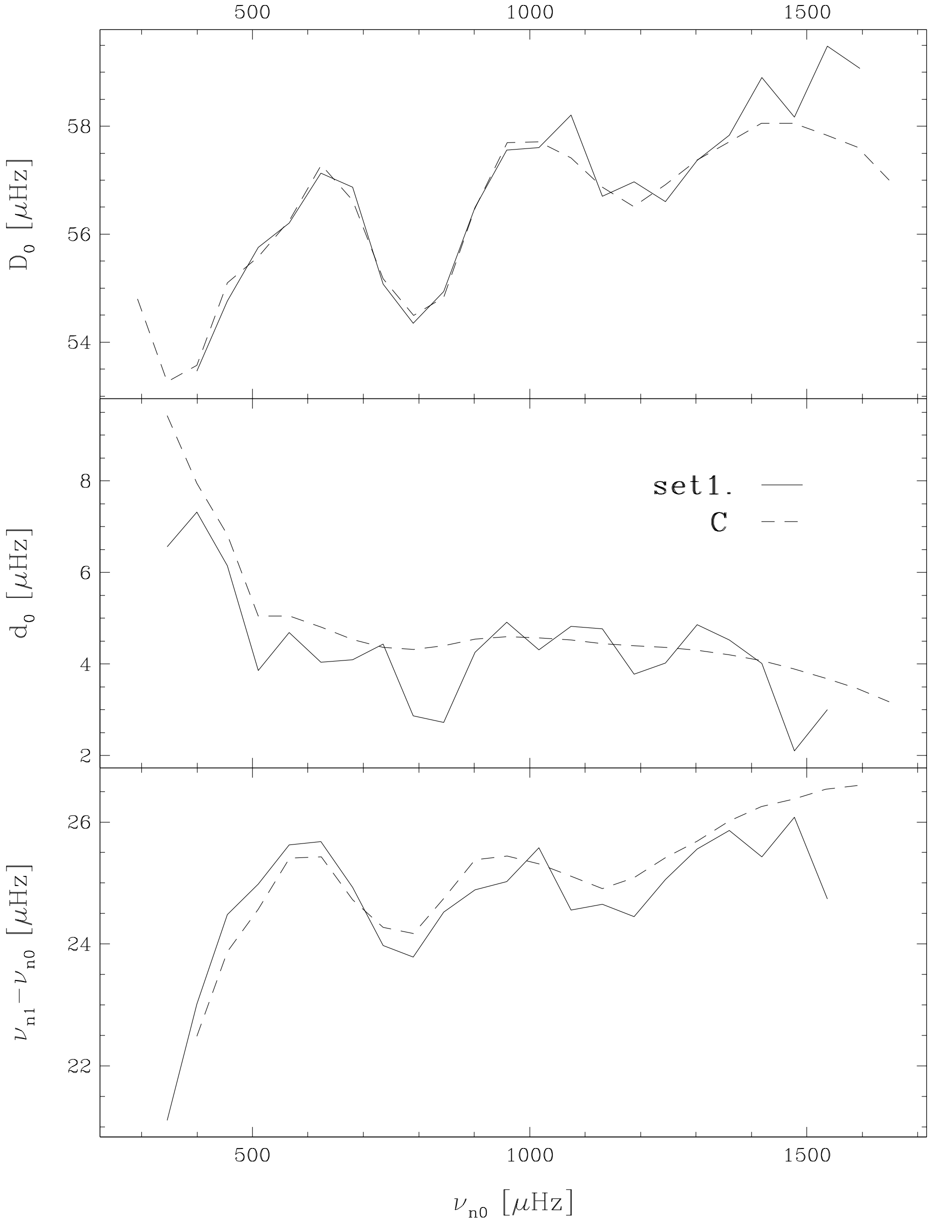

Figure 8: Large separations, small separations and $\nu_{n1} - \nu_{n0}$ for `set1` and model C. We are not able to reproduce, for example, the small separation profile observed, so far.

model	t [10^9yr]	X_c	$\log L/L_\odot$	$\log T_{eff}$	r_c/R
C^1	1.893	0.179	0.8280	3.8150	0.0583
C^1_{CESAM}	2.009	0.140	0.8182	3.8118	0.0564

Table 2: Evolutionary parameters of two models with close p-mode spectra, according to different codes.

the search (model F), reproduced well both p-mode and mixed-mode spectra. Some of its parameters coincide with true parameters kept secret so far. The mass and chemical composition are found to fit.

4.3 Uncertainties

There is also the comparison between two independent evolutionary and pulsational codes among advantages of the *hare and hound exercise*. Equipped with such tools, we are able to evaluate some intrinsic uncertainties in model parameters coming from different modeling algorithms. In our simple analysis we focused on one nonrotating model with imposed ZAMS parameters (same as for model C). Oscillation frequencies of the model coming from code1 (C^1_{CESAM}) were then reproduced using code2. Two models (C^1_{CESAM}, C^1) which p-mode spectra match (Figure 9.) were then compared. Table 2. quotes some evolutionary quantities for the models. We see that the acoustic spectra coincidence is hardly affected by the strong difference in the structure of deep interior. This difference is probably due to the adopted burning rates. The HR diagram uncertainty is illustrated in Figure 10. Similar shift between the models concerned can be reproduced by changing the imposed envelope depth for the evolutionary calculations. We claim, this might be one of important modeling parameters that should be fine-tuned to reduce modeling uncertainty. We found that opacity or equation of state errors, due to interpolation grid, are not so significant.

5 Conclusion

We are able to reproduce most of spectral features from both `set1` and `set2` using two completely different evolutionary and oscillatory codes. Our forward method of searching models that fit radial mode frequencies works well in the framework of *hare and hound*. It is obvious that our models still need to be constrained for $\ell = 1, 2$ p-modes. We claim, however, that incorporating few mixed-mode frequencies in the analysis is a useful extension, while their frequencies are very sensitive to age changes. Thus, we emphasize the advantages of choosing evolved solar-like star among targets of an asteroseismology mission.

We stress also the necessity of fine-tuning of the evolutionary parameters (for example, envelope depth). Revision of burning rates adopted is also advised in order to minimize evolutionary uncertainties. Those are sources of additional errors in any method of reproducing spectra.

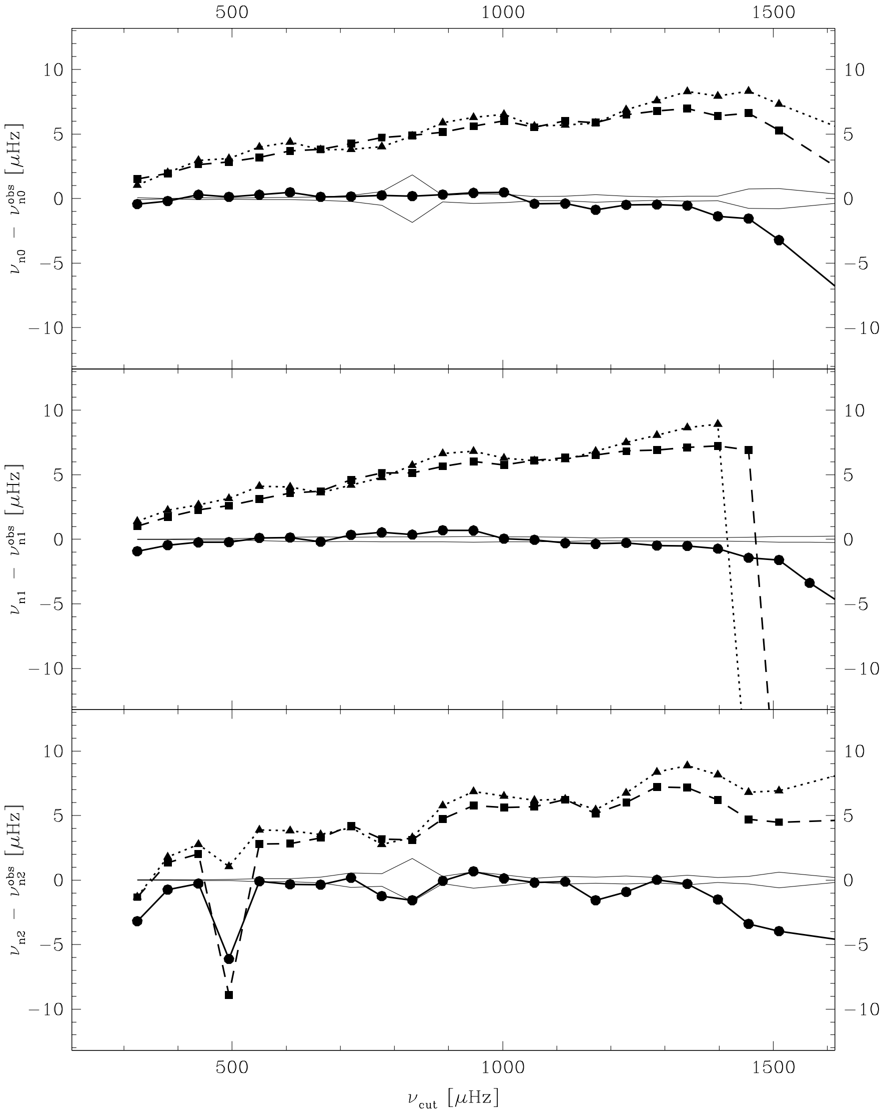

Figure 9: Model frequencies for $\ell = 0, 1, 2$ for C (dots), C^1 (squares) and C^1_{CESAM} (triangles). All frequencies are shown relative to those from `set1`. Differences in the deep interior structure are visible for mixed-modes (~ 500 μHz for $\ell = 2$).

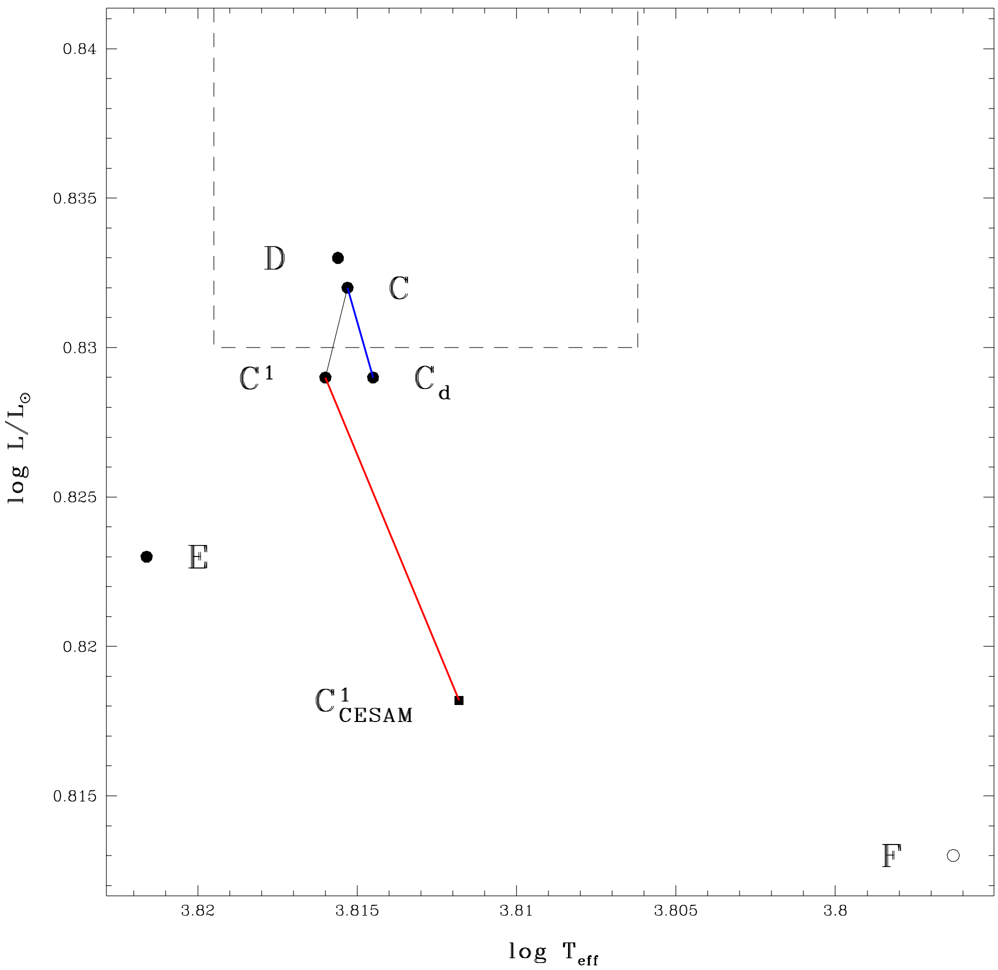

Figure 10: HR diagram positions for some discussed oscillating models. Red line connects two different models with very similar pulsational behavior. Blue line connects two models with different envelope depth (C: $M_{env}/M = 5\%$, C_d: 3%). Dashed line encompasses *hare and hound* box.

6 Acknowledgements

One of the authors (BLP) benefits grants from Polish Academy of Sciences (KBN 5P03D 030 20) and Jumelage France-Pologne.

References

[1] Baglin, A. and The COROT Team, 1998, Asteroseismology from space - The COROT Experiment, *IAU Symp. 185: New Eyes to See Inside the Sun and the Stars*, **185**, 301

[2] Bahcall, J.N. and Pinsonneault, M.H., 1995, *Rev. of Mod. Physics*, **67**, 781

[3] Grec, G., 1981, *Ph. D. thesis*, Université de Nice

[4] Provost, J., 2001, About frequency properties of solar-like stars, *COROT SWG Milestones Proceedings*, `http://dasgal.obspm.fr/~michel/MilestoneProc/SWGproc2000.html`

[5] Rogers, F.J., Swenson, F.J. and Iglesias, C.A., 1996, *Astrophys. J.*, **456**, 902

[6] Iglesias, C.A. and Rogers, F.J., 1996, *Astrophys. J.*, **464**, 943